Arcsine Laws of Light

V. G. Ramesh, K. J. H. Peters, and S. R. K. Rodriguez*
Center for Nanophotonics, AMOLF, Science Park 104, 1098 XG Amsterdam, Netherlands

(Received 14 August 2022; accepted 6 February 2024; published 25 March 2024)

We demonstrate that the time-integrated light intensity transmitted by a coherently driven resonator obeys Lévy's arcsine laws—a cornerstone of extreme value statistics. We show that convergence to the arcsine distribution is algebraic, universal, and independent of nonequilibrium behavior due to nonconservative forces or nonadiabatic driving. We furthermore verify, numerically, that the arcsine laws hold in the presence of frequency noise and in Kerr-nonlinear resonators supporting non-Gaussian states. The arcsine laws imply a weak ergodicity breaking which can be leveraged to enhance the precision of resonant optical sensors with zero energy cost, as shown in our companion manuscript [V. G. Ramesh *et al.*, companion paper, Phys. Rev. Res. (2024).]. Finally, we discuss perspectives for probing the possible breakdown of the arcsine laws in systems with memory.

DOI: 10.1103/PhysRevLett.132.133801

Random processes have fascinated physicists for decades. A seminal result due to Paul Lévy is the existence of arcsine laws for random walks and Brownian motion [1]. There are three arcsine laws, one for each of these observables: (i) the fraction of time spent above the mean, T_+; (ii) the fraction of time up to the last crossing of the mean, T_0; and (iii) the fraction of time taken to reach the maximum, T_m. For all three times $T_{j=+,0,m}$, the probability distribution $\mathcal{P}$ and cumulative distribution $\mathcal{C}$ are

$$\mathcal{P}(T_j) = \frac{1}{\pi}\frac{1}{\sqrt{T_j(1-T_j)}} \tag{1a}$$

$$\mathcal{C}(T_j) = \int_0^{T_j} \mathcal{P}(T'_j)dT'_j = \frac{2}{\pi}\arcsin\left(\sqrt{T_j}\right). \tag{1b}$$

Equation (1b) inspired the name "arcsine laws," while Eq. (1a) expresses the interesting fact that extreme deviations from the mean are likely to occur.

Arcsine laws have been studied in various physics contexts, including stochastic thermodynamics [2], polymer melting [3], interface growth [4], heterogeneous diffusion [5], and others [6–9]. Similarly, in competitive sports [10], genomics [11], and finance [12–14], arcsine laws arise. In addition, generalizations of the arcsine laws for fractional Brownian motion have drawn interest [15]. The form of the distribution Eq. (1a) has also inspired studies of wave transport through disordered media [16–20], since it corresponds to the distribution of transmission eigenvalues. In this correspondence, the so-called open and closed channels (which dominate transport [21]) are the counterparts of the extreme deviations from the mean observed in $T_{j=+,0,m}$.

Despite their pervasiveness, the arcsine laws have never been explored in coherently driven resonators. Such resonators offer a unique platform for investigating extreme value statistics and arcsine laws in hitherto unexplored regimes. In particular, we will show that the balance between conservative and nonconservative forces acting on cavity-confined light fields can be precisely controlled across an enormous range. This control enables probing the arcsine laws in systems arbitrarily driven out-of and into equilibrium. In turn, understanding the statistics of optical processes is relevant to numerous technologies where noise plays a crucial role, like sensors [22–26], beyond-von-Neumman computers [27–29], isolators [30–35], and quantum devices [36–39].

In this Letter we demonstrate that the time-integrated transmission of a coherently driven resonator obeys Lévy's arcsine laws. We first illustrate how nonconservative forces, which make the steady state nonequilibrium, can be widely and precisely controlled in a laser-driven cavity. Leveraging this capability, we experimentally evidence the arcsine laws in an adiabatic protocol with time-dependent nonconservative force. Beyond demonstrating the arcsine laws asymptotically, we analyze how the finite time cumulative distributions of $T_{+,0,m}$ converge to $\mathcal{C}(T_{j=+,0,m})$ as the integration time increases. This convergence follows a power law with a universal exponent independent of the extent of nonequilibrium behavior. Through simulations we support our findings, and further show that the arcsine laws hold: (i) for time-integrated fields as well as intensities, (ii) in nonadiabatic protocols, (iii) in the absence of a protocol, (iv) in the presence of frequency noise, and (v) in highly nonlinear regimes involving non-Gaussian steady states. Finally, we discuss why the arcsine laws imply weak ergodicity breaking. Our companion paper demonstrates the relevance of this effect to optical sensing [40]. While we focus on a laser-driven cavity, all our results should hold for any single-mode coherently driven resonator such as a

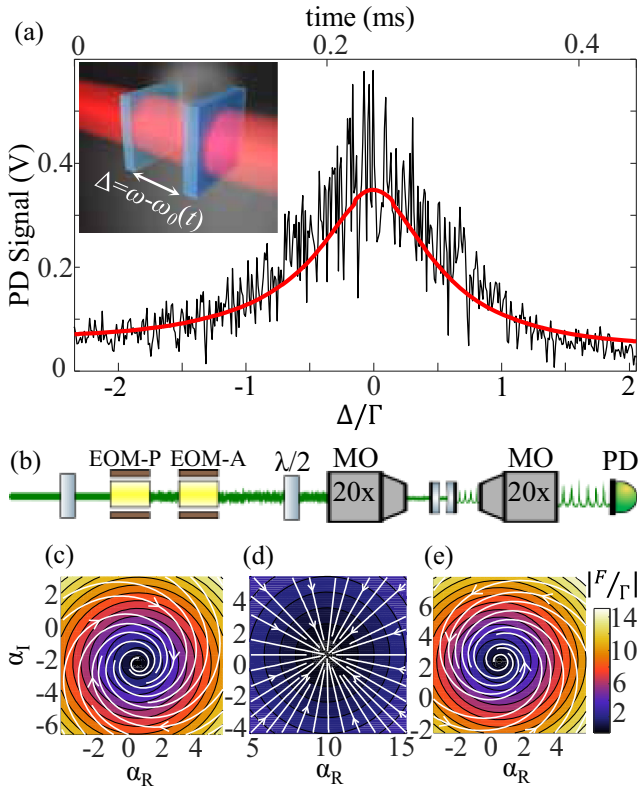

FIG. 1. (a) Inset: We use a laser-driven single-mode cavity to test the arcsine laws and study their implications for optical processes. The cavity length and hence the laser-cavity detuning Δ are periodically modulated. Main panel: Single-shot and averaged intensity transmitted through the cavity shown as a black curve and a red curve, respectively, both as a function of Δ referenced to the loss rate Γ. (b) Experimental setup for measuring the cavity transmission while adding noise to the laser amplitude and phase using electro-optic modulators EOM-A and EOM-P, respectively. MO means microscope objective and PD means photodetector. (c)–(e) Color and white arrows illustrate the force magnitude $|\vec{F}/\Gamma|$ and direction, respectively, exerted on the light field $\alpha = \alpha_R + i\alpha_I$. $A/\sqrt{\Gamma} = 7$ for all calculations, and (c) $\Delta/\Gamma = -2$, (d) $\Delta/\Gamma = 0$, and (e) $\Delta/\Gamma = 2$. The dynamics of α in (c) and (e) resemble Brownian motion in a stirred fluid.

superconducting circuit [37], a magnon cavity [41], or an acoustic resonator [42].

Our experiment involves measuring the transmission of a continuous wave laser through a plano-concave Fabry-Pérot cavity [see Fig. 1(a) inset], while periodically modulating the cavity length. We use piezoelectric actuators to align the cavity mirrors and then to modulate their distance. The planar mirror is a 50 nm thick silver layer on glass. The concave mirror (5.2 μm diameter, 6 μm radius of curvature) was made by focused ion beam milling a glass substrate [43], and subsequently depositing a distributed Bragg reflector with 99.9% reflectance at the laser wavelength 532 nm. The small radius of curvature and high mirror reflectivity strongly confine the optical modes, allowing us to probe a single mode in scans of up to ~50 resonance linewidths; we implement shorter scans of 4.5 linewidths. In this single mode limit, the light field α in our cavity satisfies

$$i\dot{\alpha} = \left(-\Delta(t) - i\frac{\Gamma}{2}\right)\alpha + i\sqrt{\kappa_L}A + D\zeta(t). \tag{2}$$

Equation (2) is written in a frame rotating at the laser frequency ω. $\Delta(t) = \omega - \omega_0(t)$ is the detuning between ω and the resonance frequency $\omega_0(t)$, which we modulate using the actuators. Modulating ω_0 is equivalent to modulating ω because their difference Δ is the relevant parameter and the cavity does not contain frequency-dependent absorption. $\Gamma = \gamma_a + \kappa_L + \kappa_R$ is the total loss rate, with γ_a the absorption rate and $\kappa_{L,R}$ input-output rates through the left or right mirror. A is the laser amplitude, assumed to be real. $D\zeta(t)$ is a complex-valued Gaussian process representing white noise, with standard deviation D, in the laser amplitude and phase. Defining $\zeta(t) = \zeta_R(t) + i\zeta_I(t)$, the noise quadratures have mean $\langle\zeta_R(t)\rangle = \langle\zeta_I(t)\rangle = 0$ and correlation $\langle\zeta_j(t')\zeta_k(t)\rangle = \delta_{j,k}\delta(t'-t)$. For our linear coherently driven system, classical and quantum descriptions are statistically equivalent [44]. Hence, Eq. (2) still holds at arbitrarily low laser intensities.

Figure 1(b) illustrates our setup, enabling fine control over every parameter in Eq. (2). We use microscope objectives with 20× magnification and 0.4 numerical aperture for light injection and transmission collection. The laser power entering the excitation objective is 1.25 mW. This power is sufficiently high to minimize the effects of detector noise, yet sufficiently low to avoid nonlinearities. The laser power is otherwise irrelevant in a linear cavity whose spectral response is power independent. The excitation path contains an amplitude and a phase modulator, each driven by a distinct waveform generator (not shown) imprinting noise on the laser. As shown in the Supplemental Material, the power spectrum of the noise is flat across several decades [45]. We implemented a 0.45 ms modulation period for Δ [see upper axis of Fig. 1(a)] to operate within this flat range, but slightly closer to the low-frequency end. Consequently, our measurements are influenced by approximately white noise. Since our protocol is much slower than the system's relaxation time $\Gamma^{-1} \sim 1$ ps, it is adiabatic. However, this has no effect on our results.

By modulating Δ we imprint a nonconservative force on α. To show this, we write $\alpha = \alpha_R + i\alpha_I$ and decompose Eq. (2) into real and imaginary parts:

$$\begin{pmatrix}\dot{\alpha_R}\\ \dot{\alpha_I}\end{pmatrix} = \underbrace{\begin{pmatrix}-\frac{\Gamma}{2} & -\Delta\\ \Delta & -\frac{\Gamma}{2}\end{pmatrix}\begin{pmatrix}\alpha_R\\ \alpha_I\end{pmatrix} + \begin{pmatrix}\sqrt{\kappa_L}A\\ 0\end{pmatrix}}_{\vec{F}/\Gamma} + D\begin{pmatrix}\zeta_R(t)\\ \zeta_I(t)\end{pmatrix}. \tag{3}$$

Equation (3) describes two-dimensional overdamped Langevin dynamics [46]. The underbraced term is the

deterministic force $\vec{F}$, divided by Γ to recover the normal form of the overdamped Langevin equation. For $\Delta = 0$, α_R and α_I decouple and $\vec{F}$ is conservative. In this case, $\vec{F}$ is irrotational, it can be derived from a purely scalar potential, the steady-state distribution of $\alpha_{R,I}$ is the equilibrium Boltzmann distribution with effective temperature given by the noise variance [47], and detailed balanced holds for $\alpha_{R,I}$ at the steady state [46]. In contrast, for $\Delta \neq 0$ $\vec{F}$ contains a nonconservative part. In that case, $\vec{F}$ is rotational, it cannot be derived from a purely scalar potential, the steady-state distribution is nonequilibrium, and detailed balance is broken [46]. Thus, our protocol with time-dependent Δ modulates the balance between conservative and nonconservative forces exerted on α.

Figures 1(c)–1(e) illustrate $\vec{F}/\Gamma$ for three values of Δ/Γ. The magnitude and direction of $\vec{F}/\Gamma$ are encoded in color and white arrows, respectively. Figures 1(c) and 1(e) correspond to values of Δ/Γ near the ends of our experimental protocol, where the laser frequency is far detuned from the cavity resonance. The spiraling field, clockwise in Fig. 1(c) and anticlockwise in Fig. 1(e), is the hallmark of a nonconservative force. At those detunings, the dynamics are analogous to Brownian motion in a stirred fluid. In contrast, Fig. 1(d) illustrates how the nonconservative force vanishes at $\Delta = 0$. All force vectors are perpendicular to the contours of constant $|\vec{F}/\Gamma|$ and point directly to the fixed point; this indicates gradient flow and equilibrium behavior.

Langevin dynamics under nonconservative forces have drawn interest in stochastic thermodynamics [46,48,49]. However, arcsine laws in those conditions have not been reported, likely because of the difficulty in controlling nonconservative forces in material systems. Our experiment therefore tests the arcsine laws in a hitherto unexplored regime where the steady state transitions between equilibrium and nonequilibrium as Δ varies.

Figure 1(a) shows measurements of the transmitted intensity when scanning the cavity length. The scan starts and ends where the nonconservative force dominates, as Figs. 1(c) and 1(e) show. The black curve is the single-shot intensity. The red curve is the intensity averaged over 200 cycles, evidencing the Lorentzian line shape characterizing a linear resonator. The single-shot intensity fluctuates because of the modulator-imprinted laser noise, which has a standard deviation that is ~80 times larger than the intrinsic laser noise.

We are interested in the transmitted intensity integrated over n modulation cycles, $\mathcal{I}_{n\tau} = \int_0^{n\tau} \kappa_R |\alpha(t)|^2 dt$ with τ the period. While $\mathcal{I}_{n\tau}$ is expressed as an integral over time, it is equivalent to an integral over frequency given that Δ depends linearly on time during our protocol. We hypothesized that arcsine laws emerge in distributions of $\mathcal{I}_{n\tau}$ as $n \to \infty$. Our hypothesis was inspired by the work of Barato *et al.*, where thermodynamic currents (e.g., the time-integrated work) were shown to obey the arcsine laws [2]. However, unlike the experiment reported in Ref. [2] where a Brownian particle experiences a purely conservative force, the light field in our cavity undergoes both conservative and nonconservative dynamics within one cycle.

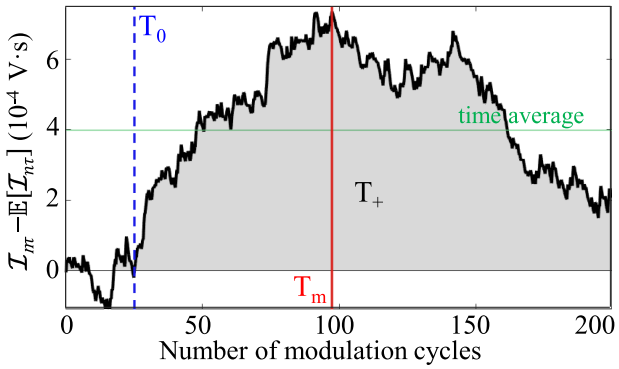

FIG. 2. Sample trajectory of the time-integrated transmitted intensity $\mathcal{I}_{n\tau}$, with the growing expectation value $\mathbb{E}[\mathcal{I}_{n\tau}]$ subtracted. The shaded area, dashed blue line, and solid red line, indicate the fractional times T_+, T_0, and T_m, respectively, to which the arcsine laws apply. The green horizontal line indicates the time average of this trajectory.

$\mathcal{I}_{n\tau}$ is obtained by consecutively integrating transmitted intensity measurements like those in Fig. 1(a). Consequently, $\mathcal{I}_{n\tau}$ is a temporally inhomogeneous process with expectation value $\mathbb{E}[\mathcal{I}_{n\tau}] = \int \mathcal{I}_{n\tau} \mathcal{P}(\mathcal{I}) d\mathcal{I}$ growing in time; $\mathcal{P}(\mathcal{I})$ is the steady-state probability distribution of $\mathcal{I}$. The growing $\mathbb{E}[\mathcal{I}_{n\tau}]$ can be regarded as a deterministic drift in the stochastic process $\mathcal{I}_{n\tau}$. By subtracting that drift, we arrive at a trajectory like the one in Fig. 2. Figure 2 also illustrates the values of $T_{+,0,m}$ for this trajectory, which are unaffected by the subtraction of $\mathbb{E}[\mathcal{I}_{n\tau}]$.

We analyzed 1000 trajectories of $\mathcal{I}_{n\tau}$, each comprising 200 cycles. The resultant probability distributions and cumulative distributions for $T_{j=+,0,m}$ are shown in Figs. 3(a) and 3(b), respectively. $\mathcal{P}(T_j)$ and $\mathcal{C}(T_j)$, given by Eqs. (1a) and (1b), respectively, are plotted under the experimental data points. The good agreement between theory and experiment demonstrates that $\mathcal{I}_{n\tau}$ obeys the arcsine laws.

To corroborate our findings and test the arcsine laws more broadly, we performed numerical simulations of Eq. (2) using the xSDPE MATLAB toolbox [50]. We considered several driving conditions, including adiabatic and nonadiabatic protocols in Δ or A, as well as fixed (Δ, A) driving conditions. As shown in the Supplemental Material [45], in every case we found distributions like those in Fig. 3. These results demonstrate that neither adiabaticity nor temporal inhomogeneity, as in our experimental protocol, are necessary conditions for the arcsine laws. In the Supplemental Material we furthermore show that the arcsine laws hold in the presence of noise in Δ, which

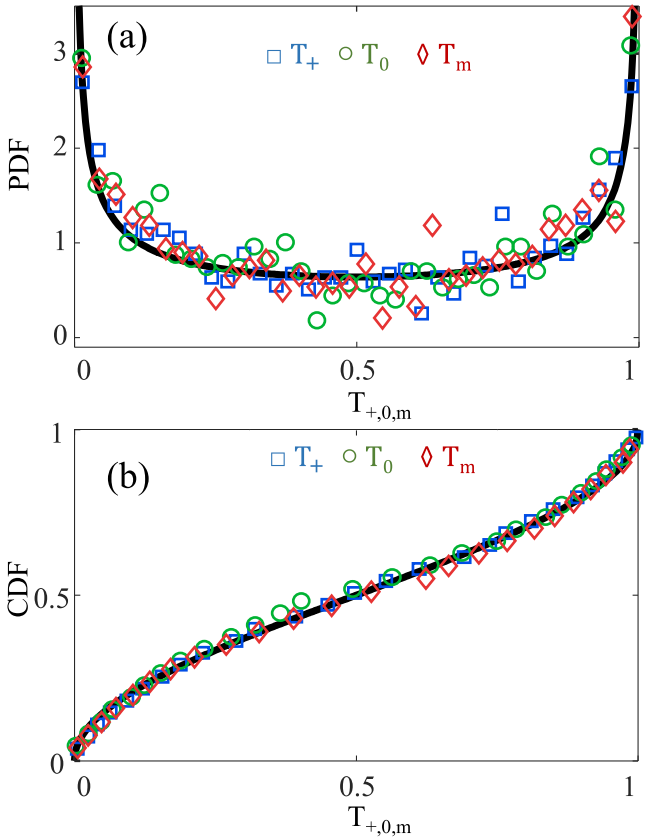

FIG. 3. (a) Probability distribution and (b) cumulative distribution for $T_{j=+,0,m}$ extracted from trajectories of the time-integrated intensity as shown in Fig. 2. Black curves in (a) and (b) are analytical predictions of Eqs. (1a) and (1b), respectively.

is multiplicative noise because it is multiplied with α. Since noise in Δ is equivalent to noise in ω, our findings demonstrate that the arcsine laws persist when the coherence of the driving laser is degraded. We furthermore analyzed the statistics of $T_{+,0,m}$ when these are obtained from the time-integrated field quadratures $\int_0^{n\tau}\alpha_R(t)dt$ and $\int_0^{n\tau}\alpha_I(t)dt$ instead of $\mathcal{I}_{n\tau}$ [45]. In those cases too, we found the arcsine laws hold [45].

We further tested the arcsine laws in simulations of a Kerr-nonlinear cavity. To that end, we added the term $U|\alpha|^2$, with U an effective photon-photon interaction strength, inside the parentheses of Eq. (2). This nonlinear term imprints a nonconservative force which, for $U > 0$, counteracts the detuning Δ in an intensity-dependent way [47]. However, unlike Δ, the Kerr nonlinearity can render the steady state non-Gaussian and squeezed, as observed in various experiments [51–54]. In the Supplemental Material we show that, even when probing such non-Gaussian and squeezed steady states nonadiabatically, the arcsine laws hold [45]. This result is relevant to fundamental studies and technologies where time-integrated signals from Kerr-nonlinear resonators are analyzed. For example, Kerr-nonlinear resonators play a central role in recent studies of dissipative phase transitions [55–65], symmetry breaking [66], polariton blockade [67,68], stochastic resonance [69,70], nonreciprocity [30,34,35,71], and sensing [25,72,73].

To study the arcsine laws beyond their asymptotic limit, we analyzed the convergence rate of the finite time cumulative distribution $\mathcal{C}_{n\tau}(T_j)$ to the arcsine distribution as the number of integrated modulation cycles increases. We quantified the convergence via the mean square residuals (MSRs), given by $(1/n)\sum[\mathcal{C}(T_j)-\mathcal{C}_{n\tau}(T_j)]^2$. Figure 4 shows the MSRs for T_+, for various driving conditions. Similar results obtained for T_0 and T_m are omitted for brevity. The purple stars are experimental data points. The black circles are the corresponding numerical results, for constant laser amplitude A and periodically modulated Δ. Numerical results for three distinct driving conditions are shown alongside. For each simulation A is modulated identically, but Δ is fixed to a different value indicated in the legend. By analyzing the MSRs for these various driving conditions, we tested whether the balance between conservative and nonconservative forces influences the convergence rate to the arcsine distribution. Remarkably, the convergence rate is always the same. The MSRs always decay by following a power law with exponent -1. Slight deviations from this behavior in experiments are likely due to frequency-dependent vibrations of our cavity mirrors; they effectively imprint colored noise in Δ that is absent in our model.

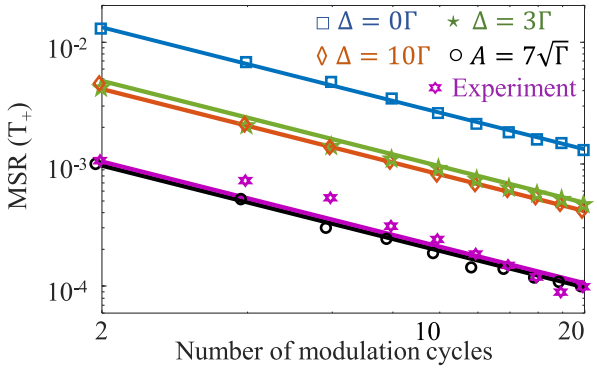

FIG. 4. Mean squared residuals between the arcsine distribution $\mathcal{C}(T_+)$ [Eq. (1b)] and the finite time distribution $\mathcal{C}_{n\tau}(T_j)$ as the transmitted intensity is integrated over an increasing number of cycles. Purple stars correspond to experiments. All other data are calculated numerically, using 10^4 simulations with distinct noise realizations per data point. Each symbol corresponds to a different protocol. Lines are power laws with exponent -1 fitted to the data. Blue squares, green stars, and orange diamonds correspond to periodic modulations of $A/\sqrt{\Gamma}$ between 5 and 12 while Δ/Γ is fixed at 0, 3, and 10 respectively. Black circles correspond to a periodic modulation of Δ/Γ between -10 and 10 while $A/\sqrt{\Gamma}=7$. $D=2\sqrt{\Gamma}$ and $\tau=50/\Gamma$ in all simulations; both choices do not alter the results.

To explain the origin of the arcsine laws, we first note that $\alpha_{R,I}(t)$ and $|\alpha(t)|^2$ are Gauss-Markov processes. Such processes do not obey the arcsine laws; only the time-integrated quantities $\int \alpha_{R,I}(t)dt$ and $\int |\alpha(t)|^2 dt$ do. Therefore, the arcsine laws cannot be ascribed to a trivial transformation of the laser noise by the cavity. Time integration crucially transforms a Gauss-Markov process into a Lévy process [74,75], for which the arcsine laws hold. In the Supplemental Material we show that the variance of the experimental time-integrated intensity $\mathcal{I}_{n\tau}$ grows linearly with time [45], as expected for a diffusive Lévy process. In addition, our companion paper [40] shows distributions of first passage and return times with power law tails. Such distributions characterize Lévy processes.

Power-law tailed distributions have a divergent first moment. For $\mathcal{I}_{n\tau}$, this means that the mean first passage and return times diverge. In this situation, where the time to explore the entire phase space and return to the mean diverges, time and ensemble averages of $\mathcal{I}_{n\tau}$ are in general different. Figure 2 illustrates this effect for a likely trajectory of $\mathcal{I}_{n\tau}$, whose time average significantly deviates from the expectation value $\mathbb{E}[\mathcal{I}_{n\tau}]$. Such differences are a signature of weak ergodicity breaking, expected in processes governed by the arcsine laws [8,76–78]. Ergodicity breaking is "weak," as opposed to "strong," when the phase space is unrestricted but the time spent in any region diverges [79]. Intuitively, we can understand this to be the case for $\mathcal{I}_{n\tau}$ by considering the first arcsine law. It states that most trajectories of $\mathcal{I}_{n\tau}$ spend most of their time far above or far below $\mathbb{E}[\mathcal{I}_{n\tau}]$. Hence, their time average will largely deviate from $\mathbb{E}[\mathcal{I}_{n\tau}]$. Ergodicity is therefore broken because, as shown in our companion paper [40], ensemble averaging over several trajectories gives a more faithful estimation of $\mathbb{E}[\mathcal{I}_{n\tau}]$ than time averaging when the total measurement time is equal. Our companion paper explores the consequences of this weak ergodicity breaking for optical sensors made of resonators such as the one studied in this Letter. We show that, given a fixed energy budget and a finite measurement time, the sensing precision of ensemble averaging can exceed that of time averaging by orders of magnitude. However, this effect disappears as the measurement time diverges and ergodicity emerges.

To conclude, we showed that the time-integrated intensity transmitted by a coherently driven resonator, $\mathcal{I}_{n\tau}$, obeys Levy's arcsine laws. As the number of considered trajectories $\mathcal{I}_{n\tau}$ increases, finite-time cumulative distributions of $T_{+,0,m}$ converge to $\mathcal{C}(T_{+,0,m})$ by following a power law with a universal exponent, regardless of nonequilibrium behavior. Fundamentally, our work demonstrates how coherently driven resonators enable probing emergent statistical structures arbitrarily far from equilibrium. For example, our optical experiment simulated two-dimensional Brownian motion in a fluid with time-dependent stirring. Implications of our results for sensing technologies, as used in biosensing [80] and LiDAR [33] for example, are discussed in our companion paper [40]. Finally, a perspective of our work is the study of emergent statistical structure in resonators with memory, such as dye-filled [81,82] and oil-filled [83,84] microcavities. In such systems, memory effects arise from the coupling of light to slow material degrees of freedom like temperature. Whether and how the arcsine laws (derived for memoryless systems) generalize to such systems is an open question.

This work is part of the research programme of the Netherlands Organisation for Scientific Research (NWO). We thank Jesse Slim, Age Tjalma, and Allard Mosk for a critical review of our manuscript, Aurelien Trichet for providing the concave mirror used in our experiments, and Christopher Jarzynski for stimulating discussions. We acknowledge funding from an ERC Starting Grant with Project No. 85269, and an Open Competition Domain Science XS Grant with file No. OCENW.XS21.1.110.

*Corresponding author: s.rodriguez@amolf.nl

[1] P. Lévy, Sur certains processus stochastiques homogènes, Compos. Math. **7**, 283 (1940).
[2] A. C. Barato, E. Roldán, I. A. Martínez, and S. Pigolotti, Arcsine laws in stochastic thermodynamics, Phys. Rev. Lett. **121**, 090601 (2018).
[3] G. Oshanin and S. Redner, Helix or coil? Fate of a melting heteropolymer, Europhys. Lett. **85**, 10008 (2009).
[4] F. Mori, S. N. Majumdar, and G. Schehr, Time between the maximum and the minimum of a stochastic process, Phys. Rev. Lett. **123**, 200201 (2019).
[5] P. Singh, Extreme value statistics and arcsine laws for heterogeneous diffusion processes, Phys. Rev. E **105**, 024113 (2022).
[6] C. Godreche and J. Luck, Statistics of the occupation time of renewal processes, J. Stat. Phys. **104**, 489 (2001).
[7] R. A. Campos, C. C. Gerry, and A. Benmoussa, Optical interferometry at the Heisenberg limit with twin Fock states and parity measurements, Phys. Rev. A **68**, 023810 (2003).
[8] A. Rebenshtok and E. Barkai, Weakly non-ergodic statistical physics, J. Stat. Phys. **133**, 565 (2008).
[9] J. Spiechowicz and J. Łuczka, Arcsine law and multistable Brownian dynamics in a tilted periodic potential, Phys. Rev. E **104**, 024132 (2021).
[10] A. Clauset, M. Kogan, and S. Redner, Safe leads and lead changes in competitive team sports, Phys. Rev. E **91**, 062815 (2015).
[11] X. Fang, H. L. Gan, S. Holmes, H. Huang, E. Peköz, A. Röllin, and W. Tang, Arcsine laws for random walks generated from random permutations with applications to genomics, J. Appl. Probab. **58**, 851 (2021).
[12] T.-C. Han and C.-M. Wang, Shipping bunker cost risk assessment and management during the coronavirus oil shock, Sustainability **13**, 4998 (2021).
[13] C. Dale and R. Workman, The arc sine law and the treasury bill futures market, Financ. Anal. J. **36**, 71 (1980).
[14] X. Guo, R. A. Jarrow, and A. de Larrard, The economic default time and the arcsine law, J. Financial Eng. **01**, 1450025 (2014).

[15] T. Sadhu, M. Delorme, and K. J. Wiese, Generalized arcsine laws for fractional Brownian motion, Phys. Rev. Lett. **120**, 040603 (2018).
[16] Y. V. Nazarov, Limits of universality in disordered conductors, Phys. Rev. Lett. **73**, 134 (1994).
[17] R. A. Jalabert, J.-L. Pichard, and C. W. J. Beenakker, Universal quantum signatures of chaos in ballistic transport, Europhys. Lett. **27**, 255 (1994).
[18] C. W. J. Beenakker, Random-matrix theory of quantum transport, Rev. Mod. Phys. **69**, 731 (1997).
[19] C. Mejía-Monasterio, G. Oshanin, and G. Schehr, Symmetry breaking between statistically equivalent, independent channels in few-channel chaotic scattering, Phys. Rev. E **84**, 035203(R) (2011).
[20] S. Rotter and S. Gigan, Light fields in complex media: Mesoscopic scattering meets wave control, Rev. Mod. Phys. **89**, 015005 (2017).
[21] J. Pendry, A. MacKinnon, and A. Pretre, Maximal fluctuations—a new phenomenon in disordered systems, Physica (Amsterdam) **168A**, 400 (1990).
[22] W. Langbein, No exceptional precision of exceptional-point sensors, Phys. Rev. A **98**, 023805 (2018).
[23] H.-K. Lau and A. A. Clerk, Fundamental limits and non-reciprocal approaches in non-Hermitian quantum sensing, Nat. Commun. **9**, 4320 (2018).
[24] N. A. Mortensen, P. A. D. Gonçalves, M. Khajavikhan, D. N. Christodoulides, C. Tserkezis, and C. Wolff, Fluctuations and noise-limited sensing near the exceptional point of parity-time-symmetric resonator systems, Optica **5**, 1342 (2018).
[25] S. R. K. Rodriguez, Enhancing the speed and sensitivity of a nonlinear optical sensor with noise, Phys. Rev. Appl. **13**, 024032 (2020).
[26] R. Duggan, S. A. Mann, and A. Alù, Limitations of sensing at an exceptional point, ACS Photonics **9**, 1554 (2022).
[27] K. P. Kalinin and N. G. Berloff, Simulating ising and n-state planar potts models and external fields with nonequilibrium condensates, Phys. Rev. Lett. **121**, 235302 (2018).
[28] O. Kyriienko, H. Sigurdsson, and T. C. H. Liew, Probabilistic solving of NP-hard problems with bistable nonlinear optical networks, Phys. Rev. B **99**, 195301 (2019).
[29] A. Opala, S. Ghosh, T. C. H. Liew, and M. Matuszewski, Neuromorphic computing in Ginzburg-Landau polariton-lattice systems, Phys. Rev. Appl. **11**, 064029 (2019).
[30] Y. Shi, Z. Yu, and S. Fan, Limitations of nonlinear optical isolators due to dynamic reciprocity, Nat. Photonics **9**, 388 (2015).
[31] S. Barzanjeh, M. Aquilina, and A. Xuereb, Manipulating the flow of thermal noise in quantum devices, Phys. Rev. Lett. **120**, 060601 (2018).
[32] S. R. K. Rodriguez, V. Goblot, N. C. Zambon, A. Amo, and J. Bloch, Nonreciprocity and zero reflection in nonlinear cavities with tailored loss, Phys. Rev. A **99**, 013851 (2019).
[33] K. Y. Yang, J. Skarda, M. Cotrufo, A. Dutt, G. H. Ahn, M. Sawaby, D. Vercruysse, A. Arbabian, S. Fan, A. Alù *et al.*, Inverse-designed non-reciprocal pulse router for chip-based lidar, Nat. Photonics **14**, 369 (2020).
[34] M. Cotrufo, S. A. Mann, H. Moussa, and A. Alù, Nonlinearity-induced nonreciprocity–part I, IEEE Trans. Microwave Theory Tech. **69**, 3569 (2021).
[35] M. Cotrufo, S. A. Mann, H. Moussa, and A. Alù, Nonlinearity-induced nonreciprocity–part II, IEEE Trans. Microwave Theory Tech. **69**, 3584 (2021).
[36] I. A. Walmsley, Quantum optics: Science and technology in a new light, Science **348**, 525 (2015).
[37] A. Blais, S. M. Girvin, and W. D. Oliver, Quantum information processing and quantum optics with circuit quantum electrodynamics, Nat. Phys. **16**, 247 (2020).
[38] K. Bai, Z. Peng, H.-G. Luo, and J.-H. An, Retrieving ideal precision in noisy quantum optical metrology, Phys. Rev. Lett. **123**, 040402 (2019).
[39] C. Panuski, D. Englund, and R. Hamerly, Fundamental thermal noise limits for optical microcavities, Phys. Rev. X **10**, 041046 (2020).
[40] V. G. Ramesh, K. J. H. Peters, and S. R. K. Rodriguez, companion paper, Phys. Rev. Res. (2024) [arXiv:2402.10791].
[41] Y.-P. Wang, G.-Q. Zhang, D. Zhang, T.-F. Li, C.-M. Hu, and J. Q. You, Bistability of cavity magnon polaritons, Phys. Rev. Lett. **120**, 057202 (2018).
[42] T. T. Koutserimpas, E. Rivet, H. Lissek, and R. Fleury, Active acoustic resonators with reconfigurable resonance frequency, absorption, and bandwidth, Phys. Rev. Appl. **12**, 054064 (2019).
[43] A. A. P. Trichet, P. R. Dolan, D. M. Coles, G. M. Hughes, and J. M. Smith, Topographic control of open-access microcavities at the nanometer scale, Opt. Express **23**, 17205 (2015).
[44] E. C. G. Sudarshan, Equivalence of semiclassical and quantum mechanical descriptions of statistical light beams, Phys. Rev. Lett. **10**, 277 (1963).
[45] See Supplemental Material at http://link.aps.org/supplemental/10.1103/PhysRevLett.132.133801 for numerical results evidencing the arcsine laws in cavities with linear and Kerr-nonlinear response, and for details about the experimental noise.
[46] V. Y. Chernyak, M. Chertkov, and C. Jarzynski, Path-integral analysis of fluctuation theorems for general Langevin processes, J. Stat. Mech. (2006) P08001.
[47] K. J. H. Peters, J. Busink, P. Ackermans, K. G. Cognée, and S. R. K. Rodriguez, Scalar potentials for light in a cavity, Phys. Rev. Res. **5**, 013154 (2023).
[48] V. Blickle, T. Speck, C. Lutz, U. Seifert, and C. Bechinger, Einstein relation generalized to nonequilibrium, Phys. Rev. Lett. **98**, 210601 (2007).
[49] S. Borlenghi, S. Iubini, S. Lepri, and J. Fransson, Entropy production for complex Langevin equations, Phys. Rev. E **96**, 012150 (2017).
[50] S. Kiesewetter, R. Polkinghorne, B. Opanchuk, and P. D. Drummond, xSPDE: Extensible software for stochastic equations, SoftwareX **5**, 12 (2016).
[51] R. E. Slusher, L. W. Hollberg, B. Yurke, J. C. Mertz, and J. F. Valley, Observation of squeezed states generated by four-wave mixing in an optical cavity, Phys. Rev. Lett. **55**, 2409 (1985).
[52] J. P. Karr, A. Baas, R. Houdré, and E. Giacobino, Squeezing in semiconductor microcavities in the strong-coupling regime, Phys. Rev. A **69**, 031802(R) (2004).
[53] G. Kirchmair, B. Vlastakis, Z. Leghtas, S. E. Nigg, H. Paik, E. Ginossar, M. Mirrahimi, L. Frunzio, S. M. Girvin, and

R. J. Schoelkopf, Observation of quantum state collapse and revival due to the single-photon Kerr effect, Nature (London) **495**, 205 (2013).
[54] T. Boulier, M. Bamba, A. Amo, C. Adrados, A. Lemaitre, E. Galopin, I. Sagnes, J. Bloch, C. Ciuti, E. Giacobino, and A. Bramati, Polariton-generated intensity squeezing in semiconductor micropillars, Nat. Commun. **5**, 3260 (2014).
[55] H. J. Carmichael, Breakdown of photon blockade: A dissipative quantum phase transition in zero dimensions, Phys. Rev. X **5**, 031028 (2015).
[56] J. M. Fink, A. Dombi, A. Vukics, A. Wallraff, and P. Domokos, Observation of the photon-blockade breakdown phase transition, Phys. Rev. X **7**, 011012 (2017).
[57] W. Casteels, R. Fazio, and C. Ciuti, Critical dynamical properties of a first-order dissipative phase transition, Phys. Rev. A **95**, 012128 (2017).
[58] S. R. K. Rodriguez, W. Casteels, F. Storme, N. Carlon Zambon, I. Sagnes, L. Le Gratiet, E. Galopin, A. Lemaître, A. Amo, C. Ciuti, and J. Bloch, Probing a dissipative phase transition via dynamical optical hysteresis, Phys. Rev. Lett. **118**, 247402 (2017).
[59] T. Fink, A. Schade, S. Höfling, C. Schneider, and A. Imamoglu, Signatures of a dissipative phase transition in photon correlation measurements, Nat. Phys. **14**, 365 (2018).
[60] F. Minganti, A. Biella, N. Bartolo, and C. Ciuti, Spectral theory of Liouvillians for dissipative phase transitions, Phys. Rev. A **98**, 042118 (2018).
[61] D. O. Krimer and M. Pletyukhov, Few-mode geometric description of a driven-dissipative phase transition in an open quantum system, Phys. Rev. Lett. **123**, 110604 (2019).
[62] D. Huybrechts and M. Wouters, Dynamical hysteresis properties of the driven-dissipative Bose-Hubbard model with a Gutzwiller Monte Carlo approach, Phys. Rev. A **102**, 053706 (2020).
[63] X. H. H. Zhang and H. U. Baranger, Driven-dissipative phase transition in a Kerr oscillator: From semiclassical $\mathcal{PT}$ symmetry to quantum fluctuations, Phys. Rev. A **103**, 033711 (2021).
[64] H. Alaeian, G. Giedke, I. Carusotto, R. Löw, and T. Pfau, Limit cycle phase and goldstone mode in driven dissipative systems, Phys. Rev. A **103**, 013712 (2021).
[65] M. Soriente, T. L. Heugel, K. Omiya, R. Chitra, and O. Zilberberg, Distinctive class of dissipation-induced phase transitions and their universal characteristics, Phys. Rev. Res. **3**, 023100 (2021).
[66] B. Garbin, A. Giraldo, K. J. H. Peters, N. G. R. Broderick, A. Spakman, F. Raineri, A. Levenson, S. R. K. Rodriguez, B. Krauskopf, and A. M. Yacomotti, Spontaneous symmetry breaking in a coherently driven nanophotonic Bose-Hubbard dimer, Phys. Rev. Lett. **128**, 053901 (2022).
[67] A. Delteil, T. Fink, A. Schade, S. Höfling, C. Schneider, and A. İmamoğlu, Towards polariton blockade of confined exciton–polaritons, Nat. Mater. **18**, 219 (2019).
[68] G. Muñoz-Matutano, A. Wood, M. Johnsson, X. Vidal, B. Q. Baragiola, A. Reinhard, A. Lemaître, J. Bloch, A. Amo, G. Nogues *et al.*, Emergence of quantum correlations from interacting fibre-cavity polaritons, Nat. Mater. **18**, 213 (2019).
[69] H. Abbaspour, S. Trebaol, F. Morier-Genoud, M. T. Portella-Oberli, and B. Deveaud, Stochastic resonance in collective exciton-polariton excitations inside a GaAs microcavity, Phys. Rev. Lett. **113**, 057401 (2014).
[70] B. Braeckeveldt and B. Maes, Temperature-induced stochastic resonance in Kerr photonic cavities for frequency shift, J. Opt. Soc. Am. B **39**, 2074 (2022).
[71] D. L. Sounas, J. Soric, and A. Alù, Broadband passive isolators based on coupled nonlinear resonances, National electronics review **1**, 113 (2018).
[72] T. L. Heugel, M. Biondi, O. Zilberberg, and R. Chitra, Quantum transducer using a parametric driven-dissipative phase transition, Phys. Rev. Lett. **123**, 173601 (2019).
[73] K. J. H. Peters and S. R. K. Rodriguez, Exceptional precision of a nonlinear optical sensor at a square-root singularity, Phys. Rev. Lett. **129**, 013901 (2022).
[74] M. Abundo, On the representation of an integrated Gauss-Markov process, Sci. Math. Jpn. **77**, 357 (2015).
[75] R. Hintze and I. Pavlyukevich, Small noise asymptotics and first passage times of integrated Ornstein–Uhlenbeck processes driven by α-stable Lévy processes, Bernoulli **20**, 265 (2014).
[76] E. Lutz, Power-law tail distributions and nonergodicity, Phys. Rev. Lett. **93**, 190602 (2004).
[77] G. Margolin and E. Barkai, Nonergodicity of blinking nanocrystals and other Lévy-walk processes, Phys. Rev. Lett. **94**, 080601 (2005).
[78] G. Bel and E. Barkai, Random walk to a nonergodic equilibrium concept, Phys. Rev. E **73**, 016125 (2006).
[79] J. P. Bouchaud, Weak ergodicity breaking and aging in disordered systems, J. Phys. I (France) **2**, 1705 (1992).
[80] F. Vollmer and S. Arnold, Whispering-gallery-mode biosensing: Label-free detection down to single molecules, Nat. Methods **5**, 591 (2008).
[81] J. Klaers, J. Schmitt, F. Vewinger, and M. Weitz, Bose–Einstein condensation of photons in an optical microcavity, Nature (London) **468**, 545 (2010).
[82] H. Alaeian, M. Schedensack, C. Bartels, D. Peterseim, and M. Weitz, Thermo-optical interactions in a dye-microcavity photon Bose–Einstein condensate, New J. Phys. **19**, 115009 (2017).
[83] Z. Geng, K. J. H. Peters, A. A. P. Trichet, K. Malmir, R. Kolkowski, J. M. Smith, and S. R. K. Rodriguez, Universal scaling in the dynamic hysteresis, and non-Markovian dynamics, of a tunable optical cavity, Phys. Rev. Lett. **124**, 153603 (2020).
[84] K. J. H. Peters, Z. Geng, K. Malmir, J. M. Smith, and S. R. K. Rodriguez, Extremely broadband stochastic resonance of light and enhanced energy harvesting enabled by memory effects in the nonlinear response, Phys. Rev. Lett. **126**, 213901 (2021).